

NANO EXPRESS

Open Access



High-Order Dielectric Metasurfaces for High-Efficiency Polarization Beam Splitters and Optical Vortex Generators

Zhongyi Guo^{1*} , Lie Zhu¹, Kai Guo¹, Fei Shen¹ and Zhiping Yin²

Abstract

In this paper, a high-order dielectric metasurface based on silicon nanobrick array is proposed and investigated. By controlling the length and width of the nanobricks, the metasurfaces could supply two different incremental transmission phases for the X-linear-polarized (XLP) and Y-linear-polarized (YLP) light with extremely high efficiency over 88%. Based on the designed metasurface, two polarization beam splitters working in high-order diffraction modes have been designed successfully, which demonstrated a high transmitted efficiency. In addition, we have also designed two vortex-beam generators working in high-order diffraction modes to create vortex beams with the topological charges of 2 and 3. The employment of dielectric metasurfaces operating in high-order diffraction modes could pave the way for a variety of new ultra-efficient optical devices.

Keywords: Metasurface, Beam splitters, Phase modulation, Optical vortices

Background

In recent years, the full control of electromagnetic waves has been an emerging area of research. For the quest to realize such control, metamaterials have attracted significant attentions for their novel physical properties, which could be artificially engineered as desired by structuring their constituents [1]. So far, metamaterials have been used to achieve many excellent optical properties, such as negative refraction, zero-refraction, and slow-light. However, three-dimensional metamaterial has many drawbacks, such as high intrinsic losses and fabrication difficulty, which restrict its real applications. With the developments of nanotechnology, two-dimensional metamaterials, or so-called metasurfaces, have been proposed to avoid these drawbacks due to their ultrathin subwavelength structures, relatively easy fabrication and conformal integrations with systems [2, 3]. Metasurfaces typically consist of an array of optical resonators with subwavelength period and function as interface discontinuities. It could introduce an abrupt change in the amplitude or phase of the impinging beam by designing the

geometry of the resonator. Based on this concept, various metasurfaces with different functions have been implemented, including tunable waveguide [4, 5], waveplates [6, 7], lens [8–11], anomalous refraction [12, 13], compact vortex generators [14–16], and high-resolution holograms [17–19].

Although metasurface exhibits much better efficiency compared with three-dimensional metamaterials, the loss should still be considered seriously due to the common use of metal. Hence, there are some improved methods to increase the transmission efficiency, including the Huygens' metasurfaces and all-dielectric metasurfaces. The Huygens' metasurfaces could avoid low efficiency; nevertheless, the fabrication of the three-dimensional structures still hinders its applications in reality [20]. Fortunately, dielectric metasurfaces could be optimized to simultaneously possess overlapping electric and magnetic resonances at the same frequencies and thus enable full 2π phase control with high transmission efficiency [21–27]. However, most of the demonstrated optical devices in the previous works use the $\pm 1st$ order diffraction modes to manipulate the wavefront of light rather than the high order modes [28–30]. Recently, a novel approach has been proposed to control the incident wavefront and operates in high order modes by

* Correspondence: guozhongyi@hfut.edu.cn

¹School of Computer and Information, Hefei University of Technology, Hefei 230009, China

Full list of author information is available at the end of the article

modulating the discrete phase; still, they obtained quite low transmission efficiencies due to the intrinsic Ohmic loss of metal [31, 32].

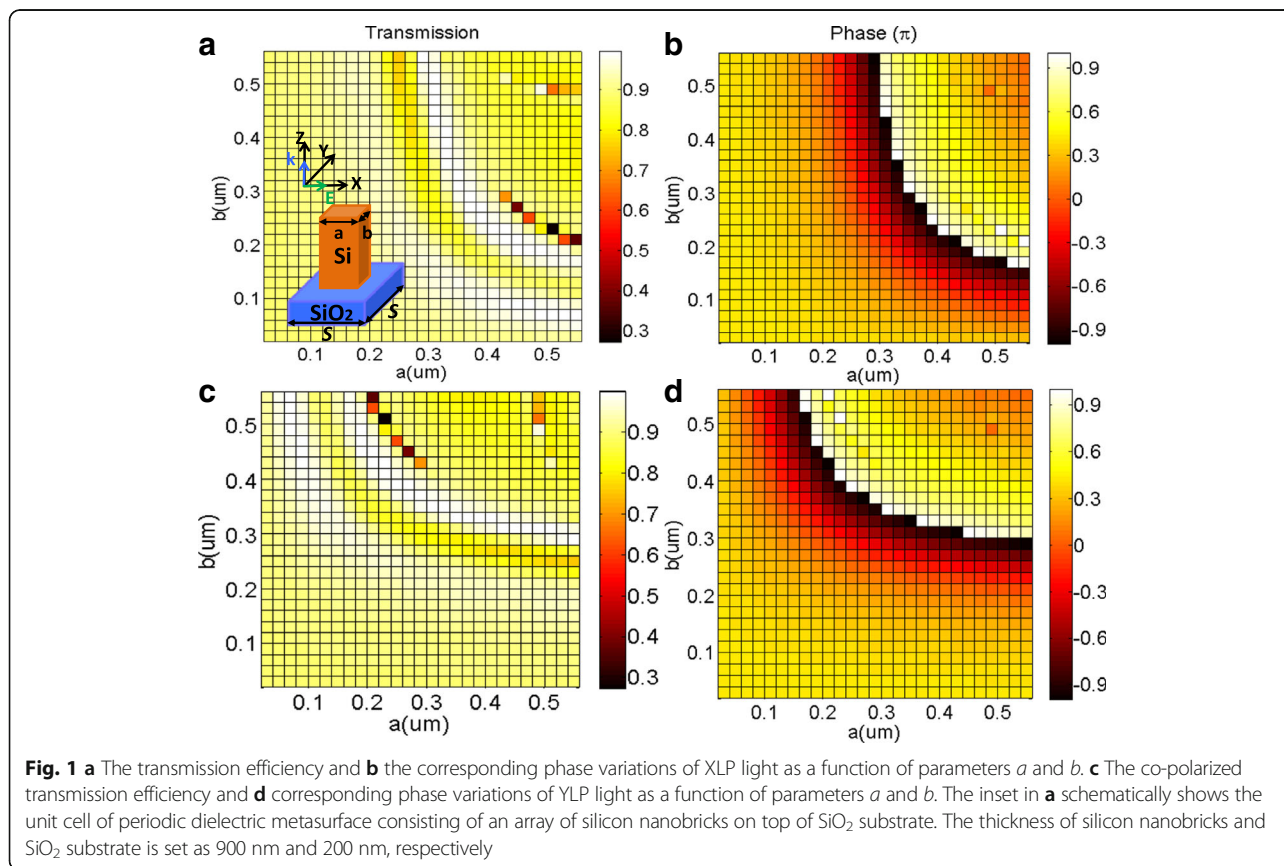
In this work, we propose a dielectric metasurface to manipulate the wavefront operating in high-order diffraction modes with extremely high transmission efficiency. Based on the proposed dielectric metasurface, two polarizing beam splitters with abrupt phase discontinuities have been designed in the telecommunication band and operating in high-order modes. The polarizing beam splitters are capable of generating two different wavefronts for two orthogonal input polarizations with extremely high efficiency up to 88%. In addition, we have also designed two vortex beam generators with the topological charges of 2 and 3 to further demonstrate the capability of the designed metasurface to manipulate light in high-order diffraction modes.

Methods

The schematic of the designed dielectric metasurfaces is shown in the inset of Fig. 1a. It is composed of 900-nm thick crystalline silicon nanobrick etched on a 200-nm thick glass substrate, whose refractive indices are 3.48 and 1.48, respectively. Due to the high refractive index, silicon exhibits high-quality resonant properties and low intrinsic ohmic losses. Furthermore, the nanostructured

silicon can be easily obtained by mature technology of semiconductor with low manufacture cost, such as EBL and FIB. The SiO_2 substrate was used due to that the reflection loss and the absorption loss can be nearly neglected in the wavelength of 1500 nm. The lattice constant is chosen as $S = 650$ nm. Thus, the geometric phase of the transmitted light induced by a silicon nanorod depends on the nanobrick dimensions along X- and Y-directions. The numerical simulation is performed by FDTD (finite-different time-domain) method. In the simulations, the perfectly matched layer (PML) was added to the layer above and below a cell to function as absorbing boundary conditions. In addition, the periodic boundary conditions (PBC) have also been applied around a cell or a unit cell. The operation wavelength is chosen to be 1500 nm for the wavelength of optical communications.

By using the numerical simulation, as depicted in Fig. 1, the co-polarized transmitted efficiency and the corresponding phase variations for both X-linear-polarized (XLP) light and Y-linear-polarized (YLP) light are calculated as functions of the geometries of the silicon bricks. When the XLP light is incident to the proposed dielectric metasurface, there is high transmittance for almost all of the nanobrick dimensions, as presented in Fig. 1a. Meanwhile, Fig. 1b implies a full range of phase from 0 to 2π in



transmission of XLP light, which could provide a full coverage of wavefront phase. More importantly, for the vast majority of dimensions, the nanobricks have over 88% co-polarized power transmission efficiency, which could be attributed to the low reflection and nearly no absorption of the dielectric metasurface at the telecommunication wavelength. The co-polarized transmission efficiency and corresponding phase variations under the YLP incidence are plotted in Fig. 1c, d, respectively. Because of the symmetry, the dependence of optical properties of dielectric metasurface on geometric dimensions for YLP light is similar with that for XLP light, which is clearly shown in Fig. 1. Hence, for YLP light, the co-polarized transmission efficiency is also higher than 88% and modulating phase range could vary from 0 to 2π .

In brief, a complete range of phase control from 0 to 2π could be effectively achieved in the case of XLP and YLP incidences by only changing the geometric dimension of nanobrick along X-direction (i.e., a) and Y-direction (i.e., b), respectively. Consequently, the range of phase control could be extended to high-order diffraction modes (i.e., from 0 to $N \times 2\pi$) due to the periodicity of phase. To demonstrate the versatility and precise phase control of the designed nanobricks, two transmission-type optical devices with high efficiency have been proposed by well designing the metasurface with simply arrangement, including two polarizing beam splitters and an optical vortex generator.

Results and discussion

Designing the Polarizing Beam Splitters

On-chip polarization control is an important issue for photonic integrated circuits. The polarizing beam splitter is one of the essential optical devices used to control the polarization on a chip, which can be used to separate the input light into two orthogonal polarization components [33, 34]. According to the simulation results above, beam splitters with steerable birefringence based on the proposed dielectric metasurface could be realized, which indicates that two different phases of XLP refraction light (ϕ_x) and YLP refraction light (ϕ_y) could be simultaneously obtained by appropriately selecting the nanobrick diameters a and b , respectively. Thus, we here design metasurfaces and employ this novel property to realize polarizing beam splitters to distinguish two orthogonal polarizations of input light to two directions with highly transmitted efficiency up to 88%. Furthermore, the designed metasurface could work in not only the first-order but also the higher-order diffraction modes.

We design the polarizing beam splitters by 13 dielectric nanobricks with three different permutations to generate different order diffraction modes with high efficiency. In the design of metasurface 1 (M_1), we discretize the phase range from 0 to 2π and from 2π to

0 into 13 nanobricks with equal step of $2\pi/13$ and $-2\pi/13$ for X- and Y-polarized transmitted light, respectively. The lateral dimensions of the 13 selected silicon nanobricks are numbered in ascending order, as shown in the first line of Fig. 2a. Apparently, the range of phase control could be extended to high-order diffraction mode by appropriately selecting the unit cells in M_1 and rearranging them. For example, if we extend the diffraction mode to the N th order, the range of phase should cover from 0 to $N \times 2\pi$ and from $N \times 2\pi$ to 0 with a phase difference of $N \times 2\pi/13$ and $-N \times 2\pi/13$ between two neighboring nanobricks for X- and Y-polarized transmitted light, respectively. Therefore, the second line of Fig. 2a presents the rearranged super cells for the third order diffraction mode (M_3), whose range of phase control is from 0 to $3 \times 2\pi$ and from $3 \times 2\pi$ to 0 with a phase difference of $3 \times 2\pi/13$ and $-3 \times 2\pi/13$ between two neighboring nanobricks for X- and Y-polarized transmitted light, respectively. In addition, the metasurface (M_5) for the fifth order diffraction mode is also constructed by a set of 13 dielectric nanobricks, which are also rearranged to cover entire range of phase control from 0 to $5 \times 2\pi$ and from $5 \times 2\pi$ to 0 with a phase difference of $5 \times 2\pi/13$ and $-5 \times 2\pi/13$ between two neighboring nanobricks for X- and Y-polarized transmitted light, respectively, as presented in the third line of Fig. 2a. In order to show the idea clearly, the transmission phases of the 13 antennas in three concrete permutations under XLP and YLP light are plotted in Fig. 2b.

In addition, the transmissions of the 13 designed nanobricks under XLP and YLP light have been simulated and agree well with the theoretical prediction. Fig. 2c shows the geometrical dimensions of the silicon nanobricks and the transmitted efficiencies of the 13 nanobricks in metasurface M_1 under XLP and YLP light. The co-polarized transmissions of most dielectric nanobricks are comparable and remain over 88% though there are two nanobricks' transmissions keeping nearly 80%. These simulation results verify that our designed metasurfaces could be applied to fabricate numerous optical devices with high efficiency.

Numerical simulations of polarizing beam splitter are performed by illuminating the designed metasurfaces M_1 at normal incidence with the polarized angle of 45° . The concrete XLP and YLP light could be extracted from the whole transmitted fields, as plotted in Fig. 3a. It is clear that there exists a well-defined wavefront and the co-polarized transmitted efficiencies of M_1 are plotted as functions of transmitted angle in Fig. 3b. The peak co-polarized transmitted angles are -10.2° and 10.2° for transmitted XLP and YLP lights, respectively. The efficiencies of the first order are $T_{xx} = 85.9\%$ and $T_{yy} = 88.4\%$ for the transmitted XLP and YLP lights, respectively, where T_{xx} is the simulated transmission coefficient of

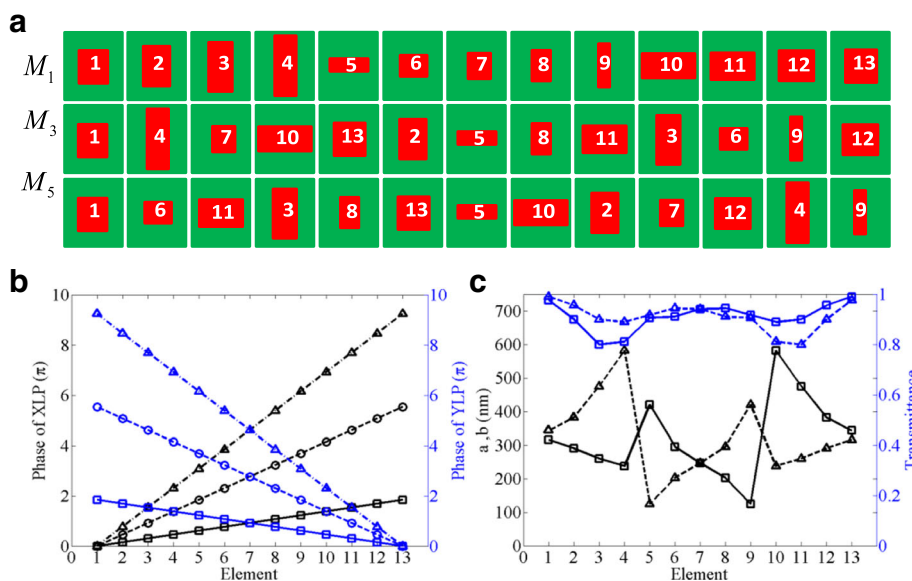
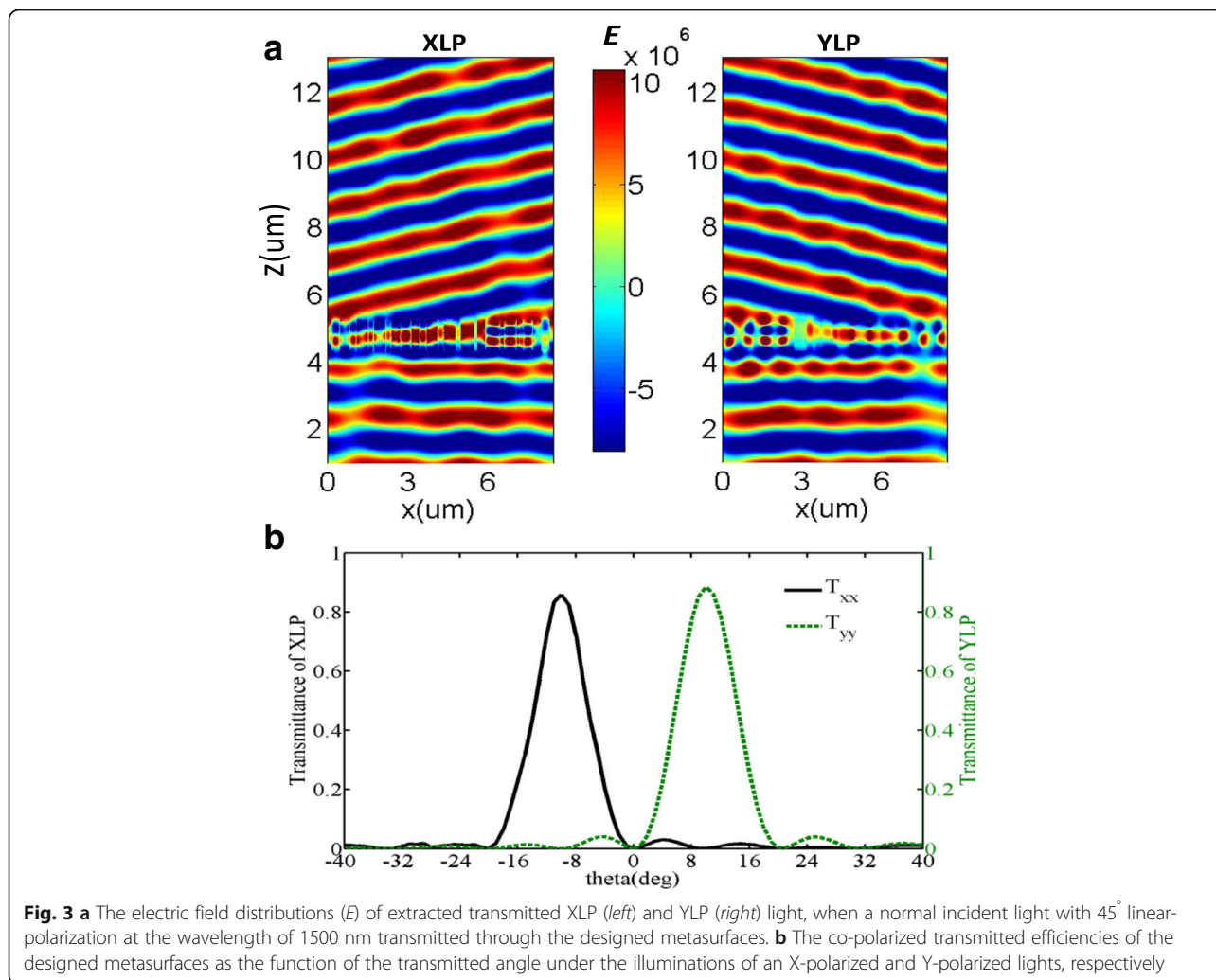


Fig. 2 Design of the dielectric metasurfaces with three different order diffraction modes. **a** Schematics of lateral dimensions of the 13 designed nanobricks. First line M_1 : a supercell with transmitted phase ranging from 0 to 2π . Second line M_3 : a rearranged super cell with phase ranging from 0 to $3 \times 2\pi$. Third line M_5 : a rearranged super cell with phase ranging from 0 to $5 \times 2\pi$. **b** The simulated transmission phases of the 13 designed nanobricks of three different modes under XLP (black lines) and YLP (blue lines) incidences, respectively. **c** **a** (black solid lines) and **b** (black dotted lines) of the 13 nanobricks used in the designed metasurfaces M_1 . The blue lines represent the transmitted efficiencies of the 13 nanobricks in M_1 under XLP (solid lines) and YLP (dotted lines) incidences, respectively

XLP light with the XLP incidence and T_{yy} is the simulated transmission coefficient of YLP light with the YLP incidence. Compared to the transmitted efficiency of the spatially homogeneous nanobrick arrays, the conversion efficiency is slightly reduced owing to the coupling between resonators with different dimensions [35]. On the basis of the generalized Snell's law, the diffraction angle of incident light at a gradient metasurface can be calculated by $\theta_t = \sin^{-1}[(\lambda_0/n_t L) + n_i \sin(\theta_i)/n_t]$, where n_t and n_i are the refractive indexes of the media in the transmission and incident sides of the interface, respectively, θ_i is the incident angle, λ_0 is the wavelength of light in vacuum, and L is the length of a supercell [36]. Thus, the theoretical results of the first order diffraction angles are $\pm 10.22^\circ$. Numerical simulation and theory agree well with each other. That is to say the designed device can serve as a polarizing beam splitter with a proper successive treatment. Furthermore, the incident wavefront has almost not been affected by the reflection light from the metasurface, which verifies that all of the incident light could be transmitted from the metasurfaces with extremely high efficiency.

For comparison, Fig. 4 shows the concrete XLP and YLP transmitted electric field distributions of the other two rearranged dielectric metasurfaces made of new designed supercells (M_3 and M_5) under the 45° linear-polarized incident light. Since the transmitted phase

range of the two supercells has been changed, the diffraction angles of M_3 and M_5 are theoretically calculated to be $\pm 32.18^\circ$ and $\pm 62.56^\circ$, respectively. In Fig. 4a, b, there exist two well-defined phase fronts with the third order diffraction angles of -32° and 32° for transmitted XLP and YLP lights, respectively. In Fig. 4c, d, the fifth order diffraction angle is -63° and 63° for transmitted XLP and YLP lights, respectively. Furthermore, the simulated co-polarized transmitted efficiencies of the designed metasurfaces composed of rearranged supercell M_3 and M_5 have also been illustrated in Fig. 5a, b, respectively. The peak transmitting angles match well with the theoretical diffraction angles calculated by the generalized Snell's law, and the co-polarized diffraction efficiencies of the third order are 82 and 84% for transmitted XLP and YLP lights. However, the co-polarized diffraction efficiencies of the fifth order are just 73.5 and 78.4% for transmitted XLP and YLP lights, which is essentially caused by the undesired EM coupling between neighboring nanobricks with different geometries. Therefore, the designed metasurfaces could work well in higher-order diffraction modes by just modifying the arrangement of the 13 dielectric nanobricks. More importantly, it is demonstrated that the diffraction mode could be customized by controlling the phase difference between adjacent dielectric nanobricks in a supercell.



Designing the Optical Vortex Generators

The optical vortex beam has a helical wavefront and carries an orbital angular momentum of $l\hbar$ [37, 38], which make it show great promises in high-resolution lithography [39, 40], optical trapping [41, 42], optical communication [43, 44], and so on. Here, the topological charge l is the number of twists of the wavefront and \hbar is the reduced Planck constant. The vortex beam with the topological charge of 1 can be generated by metasurfaces with spiral phase profile ranging from 0 to 2π with identical phase increment along the azimuthal direction. Therefore, to further demonstrate the capability of the designed metasurface to manipulate the transmitted phase and diffraction mode, we design a vortex generator that can convert an incident homogeneous Gaussian beam into a vortex beam. To achieve this goal, we arrange the 13 dielectric nanobricks of M_1 into the 13 sectors to introduce a gradient phase increment of $2\pi/13$ across the azimuthal direction. The transmitted intensity profiles under XLP incidence at $z = 10 \mu\text{m}$ are

shown in Fig. 6a and have the characteristic intensity minimum at the center corresponding to a phase singularity. The spatial phase patterns with an evident abrupt phase jump from $-\pi$ to π within a 2π azimuthal range are shown in Fig. 6d, which indicates that the topological charge of the optical devices in Fig. 6d is 1.

In addition, we design other two vortex generators to generate vortex beams by changing the arrangement of the nanobricks in M_1 . These two vortex beam generators possess the topological charges of 2 and 3, respectively. Their transmitted intensity profiles under XLP incidence are shown in Fig. 6b, c, respectively. The concrete design approaches are modulating the phase difference of the nanobricks to be $4\pi/13$ and $6\pi/13$ between two neighboring dielectric nanobricks, which are defined as M_2 and M_3 . Therefore, the instantaneous spatial phase profiles in Fig. 6e, f possess two and three evident abrupt phase jumps from $-\pi$ to π , respectively. Switching the incident polarization from XLP to YLP does not change the output intensity pattern, but the twisting direction of

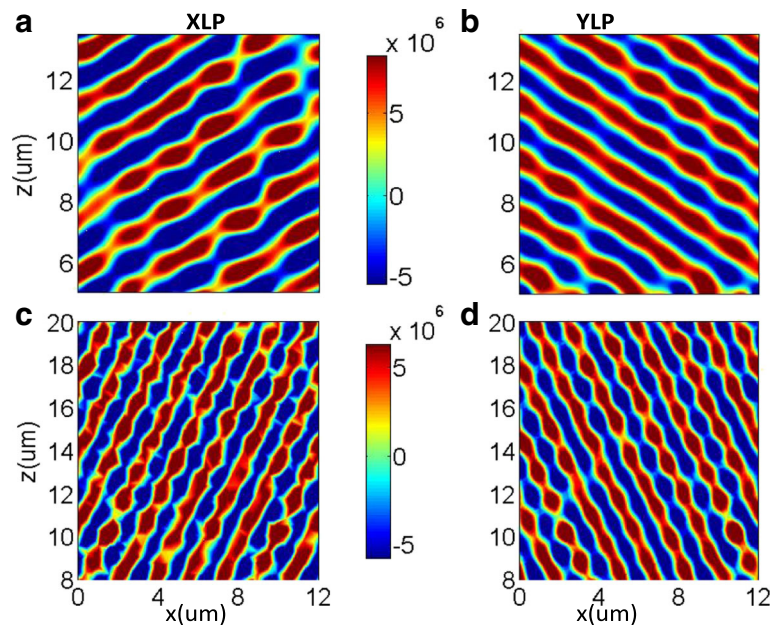


Fig. 4 The electric field distributions of extracted transmitted XLP (left) and YLP (right) under the normal incidence of 45° linear-polarization light to the metasurfaces of M_3 (a, b) and M_5 (c, d), respectively

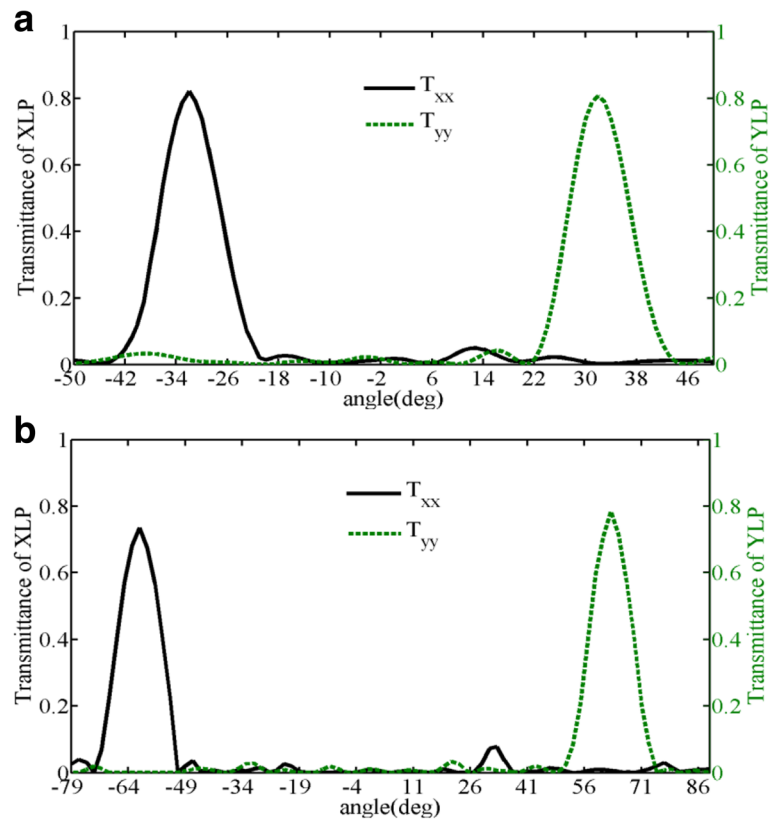
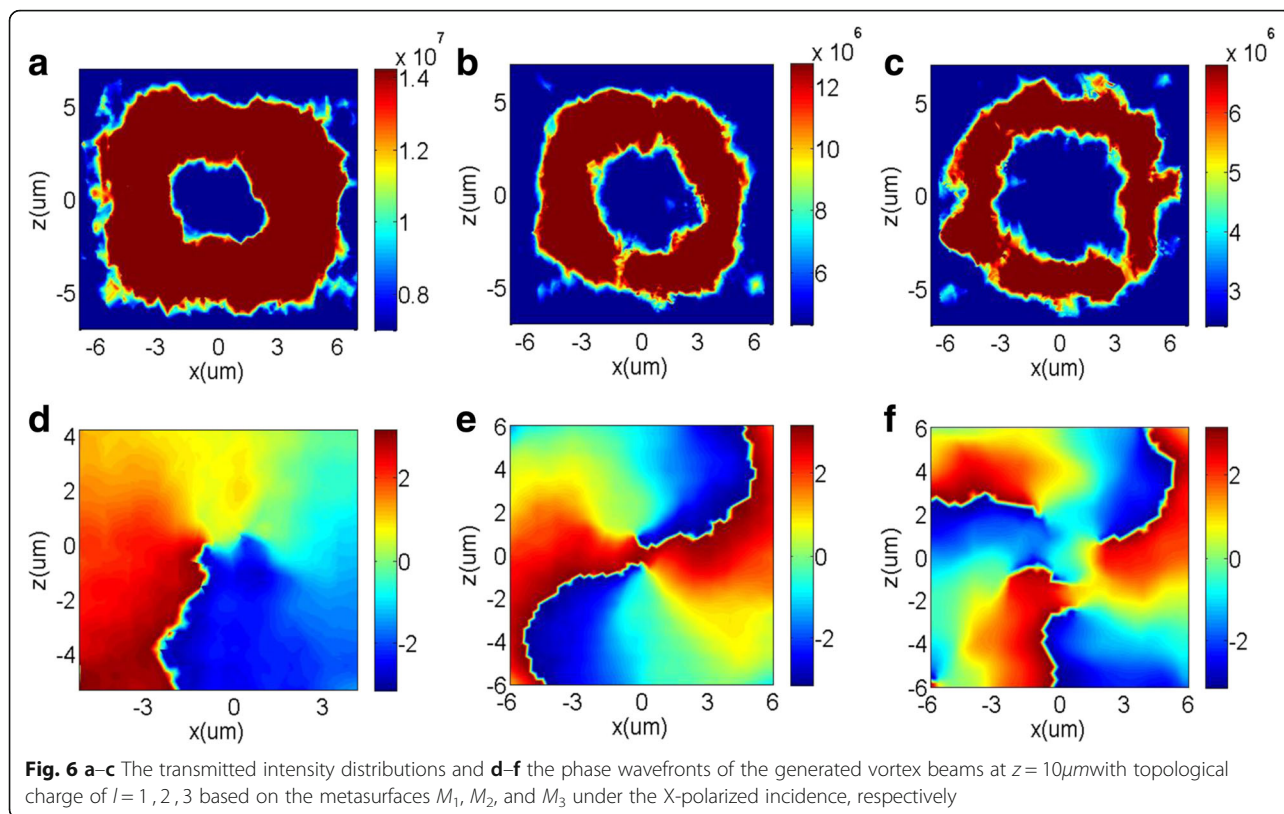


Fig. 5 The co-polarized transmitted efficiencies of the designed metasurfaces composed of rearranged supercell **a** M_3 and **b** M_5 as functions of the transmitted angle under the illumination of a X-polarized and Y-polarized light, respectively



the helical wavefront will be reverse due to the diminishing phase difference between the neighboring nanobricks. Furthermore, it should be noted that the higher-order phase profiles could also be generated by our designed dielectric metasurfaces.

Conclusions

In conclusion, we have demonstrated dielectric gradient metasurfaces consist of periodic arrangement of differently sized silicon nanobricks, which could transmit the input light with full range of manipulating phase from 0 to 2π and extremely high efficiency (over 88%) at telecommunication wavelength. Based on the designed dielectric metasurfaces, novel polarizing beam splitters working in the higher order diffraction modes are proposed to separate two orthogonal input polarized lights to arbitrary different directions. In addition, we have also designed two vortex beam generators working in the higher-order diffraction modes with different topological charges. Our work could also easily be extended to the design of other optical transmitting devices with high efficiency.

Acknowledgements

The authors gratefully acknowledge the financial supports for this work from the National Natural Science Foundation of China (No. 61775050 and No. 11505043), and Fundamental Research Funds for the Central Universities (JD2017JGPY0005).

Authors' Contributions

This manuscript is written by ZYG and LZ. The simulation is carried out by ZYG and LZ. The analysis and discussion of these obtained results are carried out by ZYG, LZ, KG, FS, and ZPY. All authors read and approved the final manuscript.

Competing Interests

The authors declare that they have no competing interests.

Publisher's Note

Springer Nature remains neutral with regard to jurisdictional claims in published maps and institutional affiliations.

Author details

¹School of Computer and Information, Hefei University of Technology, Hefei 230009, China. ²Academy of Opto-Electronic Technology, Hefei University of Technology, Hefei 230009, China.

Received: 15 July 2017 Accepted: 18 August 2017

Published online: 29 August 2017

References

- Malureanu R, Sun W, Zalkovskij M, He Q, Zhou L, Jepsen PU, Lavrinenko A (2015) Metamaterial-based design for a half-wavelength plate in the terahertz range. *Applied Physics A* 119(2):467–473
- Iyer PP, Butakov NA, Schuller JA (2015) Reconfigurable semiconductor phased-array metasurfaces. *ACS Photonics* 2(8):1077–1084
- Wang W, Guo ZY, Li RZ, Zhang JR, Li Y, Wang XS, Qu SL (2015) Ultra-thin, planar, broadband, dual-polarity plasmonic metalens. *Photonics Research* 3(3):68–71
- Minowa Y, Nagai M, Tao H, Fan K, Strikwerda AC, Zhang X, Averitt RD, Tanaka K (2011) Extremely thin metamaterial as slab waveguide at terahertz frequencies. *IEEE Transactions on Terahertz Sci Technol* 1(2):441–449

5. Wang J, Wang X, Shao H, Hu ZD, Zheng G, Zhang F (2017) Peak modulation in multicavity-coupled graphene-based waveguide system. *Nanoscale Res Lett* 12:9. doi:10.1186/s11671-016-1791-0
6. Yu N, Aieta F, Genevet P, Kats MA, Gaburro Z, Capasso F (2012) A broadband, background-free quarter-wave plate based on plasmonic metasurfaces. *Nano Lett* 12(12):6328–6333
7. Wang D, Zhang L, Gong Y, Jian L, Venkatesan T, Qiu CW, Hong M (2016) Multiband switchable terahertz quarter-wave plates via phase-change metasurfaces. *IEEE Photonics Journal* 8(1):1–8
8. Wang W, Guo ZY, Zhou KY, Sun YX, Shen F, Li Y, Qu SL, Liu ST (2015) Polarization-independent longitudinal multi-focusing metalens. *Opt Express* 23(23):29855–29866
9. Wang S, Wang X, Kan Q, Ye J, Feng S, Sun W, Han P, Qu S, Zhang Y (2015) Spin-selected focusing and imaging based on metasurface lens. *Opt Express* 23(20):26434–26441
10. Li RZ, Guo ZY, Wang W, Zhang JR, Zhang AJ, Liu JL, Qu SL, Gao J (2015) Arbitrary focusing lens by holographic metasurface. *Photonics Res* 3(5):252–255
11. Shao H, Wang J, Liu D, Hu ZD, Xia X, Sang T (2017) Plasmonic planar lens based on slanted nanoslit array. *Plasmonics* 12(2):361–367
12. Sun S, Yang K-Y, Wang C-M, Juan T-K, Chen WT, Liao CY, He Q, Xiao S, Kung W-T, Guo G-Y, Zhou L, Tsai DP (2012) High efficiency broadband anomalous reflection by gradient meta-surfaces. *Nano Lett* 12:6223–6229
13. Pors A, Albrektsen O, Radko IP, Bozhevolnyi SI (2013) Gap plasmon-based metasurfaces for total control of reflected light. *Sci Rep* 3:2155. doi:10.1038/srep02155
14. Wang W, Guo ZY, Sun YX, Shen F, Li Y, Liu Y, Wang XS, Qu SL (2015) Ultra-thin optical vortex phase plate based on the L-shaped metasurface for both linear and circular polarized incidences. *Opt Commun* 355:321–325
15. Mehmood MQ, Mei S, Hussain S, Huang K, Siew SY, Zhang L, Zhang T, Ling X, Liu H, Teng J, Danner A, Zhang S, Qiu C (2015) Visible-frequency metasurfaces for broadband anomalous reflection and high-efficiency spectrum splitting. *Nano Lett* 15(3):1615–1621
16. Mehmood MQ, Mei S, Hussain S, Huang K, Siew SY, Zhang L, Zhang T, Ling X, Liu H, Teng J, Danner A, Zhang S, Qiu C (2016) Visible-frequency metasurface for structuring and spatially multiplexing optical vortices. *Adv Mater* 28:2533–2539
17. Zheng G, Mühlenbernd H, Kenney M, Li G, Zentgraf T, Zhang S (2015) Metasurface holograms reaching 80% efficiency. *Nature Nanotechnol* 10(4):308–312
18. Huang L, Chen X, Mühlenbernd H, Zhang H, Chen S, Bai B, Tan Q, Jin G, Cheah K, Qiu C, Li J, Zentgraf T, Zhang S (2013) Three-dimensional optical holography using a plasmonic metasurface. *Nat Commun* 4:2808. doi:10.1038/ncomms3808
19. Chen WT, Yang KY, Wang CM, Huang YW, Sun G, Chiang ID, Liao CY, Hsu WL, Lin HT, Sun S, Zhou L, Liu AQ, Tsai DP (2013) High-efficiency broadband meta-hologram with polarization-controlled dual images. *Nano Lett* 14(1):225–230
20. Chen K, Feng Y, Monticone F, Zhao J, Zhu B, Jiang T, Zhang L, Kim Y, Ding X, Zhang D, Alù A, Qiu C (2017) A reconfigurable active Huygens' metalens. *Adv Mater* 29:1606422. https://doi.org/10.1002/adma.201606422
21. Asadchy V, Albooyeh M, Tretyakov S (2016) Optical metamirror: all-dielectric frequency-selective mirror with fully controllable reflection phase. *JOSA B* 33(2):A16–A20
22. Guo Z, Zhu L, Shen F, Zhou H, Gao R (2017) Dielectric metasurface based high-efficiency polarization splitters. *RSC Adv* 7(16):9872–9879
23. Shalaev MI, Sun J, Tsukernik A, Pandey A, Nikolskiy K, Litchinitser NM (2015) High-efficiency all-dielectric metasurfaces for ultracompact beam manipulation in transmission mode. *Nano Lett* 15:6261–6266
24. Arbabi A, Horie Y, Bagheri M, Faraon A (2015) Dielectric metasurfaces for complete control of phase and polarization with subwavelength spatial resolution and high transmission. *Nature Nano* 10(11):937–943
25. Guo Z, Tian L, Shen F, Zhou H, Guo K (2017) Mid-infrared polarization devices based on the double-phase modulating dielectric metasurface. *J Phys D Appl Phys* 50:254001. https://doi.org/10.1088/1361-6463/aa6f9b
26. Lin D, Fan P, Hasman E, Brongersma ML (2014) Dielectric gradient metasurface optical elements. *Science* 345(6194):298–302
27. Huang K, Dong Z, Mei S, Zhang L, Liu Y, Liu H, Zhu H, Teng J, Lukyanchuk B, Yang JKW, Qiu CW (2016) Silicon multi-meta-holograms for the broadband visible light. *Laser Photonics Rev* 10(3):500–509
28. Yue F, Wen D, Xin J, Gerardot BD, Li J, Chen X (2016) Vector vortex beam generation with a single plasmonic metasurface. *ACS photonics* 3(9):1558–1563
29. Pors A, Nielsen MG, Bozhevolnyi SI (2015) Plasmonic metagratings for simultaneous determination of Stokes parameters. *Optica* 2(8):716–723
30. Yang Y, Wang W, Moitra P, Kravchenko II, Briggs DP, Valentine J (2014) Dielectric meta-reflectarray for broadband linear polarization conversion and optical vortex generation. *Nano Lett* 14(3):1394–1399
31. Xie Y, Wang W, Chen H, Konneker A, Popa BI, Cummer SA (2014) Wavefront modulation and subwavelength diffractive acoustics with an acoustic metasurface. *Nat Commun* 5:5553. https://doi.org/10.1038/ncomms6553
32. Li Z, Hao J, Huang L, Li H, Xu H, Sun Y, Dai N (2016) Manipulating the wavefront of light by plasmonic metasurfaces operating in high order modes. *Opt Express* 24(8):8788–8796
33. Pérez-Galacho D, Halir R, Ortega-Moñux A, Alonso-Ramos C, Zhang R, Runge P, Janiak K, Bach H-G, Steffan AG, Molina-Fernández I (2013) Integrated polarization beam splitter with relaxed fabrication tolerances. *Opt Express* 21(12):14146–14151
34. Sun X, Aitchison JS, Mojahedi M (2017) Realization of an ultra-compact polarization beam splitter using asymmetric MMI based on silicon nitride/silicon-on-insulator platform. *Opt Express* 25(7):8296–8305
35. Liu S, Noor A, Du LL, Zhang L, Xu Q, Luan K, Wang TQ, Tian Z, Tang WX, Han JG, Zhang WL, Zhou XY, Cheng Q, Cui TJ (2016) Anomalous refraction and nondiffractive Bessel-beam generation of terahertz waves through transmission-type coding metasurfaces. *ACS Photonics* 3(10):1968–1977
36. Yu N, Genevet P, Kats MA, Aieta F, Tetienne JP, Capasso F, Gaburro Z (2011) Light propagation with phase discontinuities: generalized laws of reflection and refraction. *Science* 334(333):333–337
37. Yan Y, Xie G, Lavery MP, Huang H, Ahmed N, Bao C, Ren Y, Cao Y, Li L, Zhao Z, Molisch AF, Tur M, Padgett MJ, Willner AE (2014) High-capacity millimetre-wave communications with orbital angular momentum multiplexing. *Nat Commun* 5:4876. doi:10.1038/ncomms5876
38. Wang W, Li Y, Guo Z, Li R, Zhang J, Zhang A, Qu S (2015) Ultra-thin optical vortex phase plate based on the metasurface and the angular momentum transformation. *J Opt* 17(4):045102. doi:10.1088/2040-8978/17/4/045102
39. Kang M, Chen J, Wang XL, Wang HT (2012) Twisted vector field from an inhomogeneous and anisotropic metamaterial. *J Opt Soc Am B* 29:572–576
40. Bauer T, Orlov S, Peschel U, Banzer P, Leuchs G (2013) Nanointerferometric amplitude and phase reconstruction of tightly focused vector beams. *Nat Photonics* 8:23–27
41. Ng J, Lin ZF, Chan CT (2010) Theory of optical trapping by an optical vortex beam. *Phys Rev Lett* 104:103601. doi:10.1103/PhysRevLett.104.103601
42. Zhu L, Guo Z, Xu Q, Zhang J, Zhang A, Wang W, Liu Y, Li Y, Wang X, Qu S (2015) Calculating the torque of the optical vortex tweezer to the ellipsoidal micro-particles. *Opt Commun* 354:34–39
43. D'Ambrosio V, Nagali E, Walborn SP, Aolita L, Slussarenko S, Marrucci L, Sciarrino F (2012) Complete experimental toolbox for alignment-free quantum communication. *Nat Commun* 3:961. doi:10.1038/ncomms1951
44. Kai C, Huang P, Shen F, Zhou H, Guo Z (2017) Orbital angular momentum shift keying based optical communication system. *IEEE Photonics Journal* 9(2):1–10

Submit your manuscript to a SpringerOpen® journal and benefit from:

- Convenient online submission
- Rigorous peer review
- Open access: articles freely available online
- High visibility within the field
- Retaining the copyright to your article

Submit your next manuscript at ► springeropen.com